Crack detection in frozen soils using infrared camera

Yang Zhao[a], Rui Li[a], Hyungjoon Seo[a]

[a] Civil Engineering Department, Xi'an Jiaotong-Liverpool University, Suzhou, China
Email: Yang.Zhao@xjtlu.edu.cn 278154553@qq.com Hyunjoon.Seo@xjtlu.edu.cn

Abstract: Frozen soils are encountered on construction site in the polar regions or where artificial frozen ground (AFG) method is used. Thus, efficient ways to monitor the behaviour and potential failure of frozen soils are on demand. The advance in thermographic technology presented an alternative solution as the deformation occurred in frozen soil would generate inter-particle friction heat, and hence increase in temperature. In this research, uniaxial compression tests were conducted on cylindrical frozen soil specimens of three types, namely clay, sand and gravel. During the tests, the surface temperature profiles of the specimens were recorded by an infrared video camera. The thermographic videos were analysed, and the results shows that temperature increase caused by frictional heat can be observed in all three frozen soil specimens. Therefore, such temperature increase can be deemed as an indicator for the potential failure of frozen soil and such method is applicable for monitoring purpose.

Key words-
Frozen soil; Infrared camera; Crack

1   Introduction

Historically, human has been living and building structures on frozen ground in arctic area where the annually average temperature is below the freezing point of water. And artificial frozen ground (AFG) method has gained its popularity as a technique to stabilise soil during excavation recently. Due bonding effect of ice, frozen soil is more rigid and stronger than normal soil and may demonstrate mechanical behaviour similar to concrete. The crack initiation and propagation in concrete has been studied by many researchers, but few studies are focused on cracks of frozen soil.

As crack occurs, there is relative movement of soil particles around the crack, and hence frictional heat. The frictional heat may cause temperature increase, which can be observed using thermographic devices such as an infrared camera.

Researchers successfully used infrared camera to detect phenomenon with temperature changes, such as oil product spreading on water surface [1], wild fire [2], and wind flow[3].

Specifically, thermographic technique has been applied to defection in structures. Seo and Choi [4] detected crack formation in pillars using infrared camera. Though in some cases, the defection does not generate temperature change when the structure is at rest. When heated by external source, defections will show different temperature comparing to the rest of structure. Broberg [5] used infrared camera to detect defection in welds based on temperature difference between defection and its surrounding surface while the weld was heated by a flash lamp as an external IR source. Štarman and Matz [6]observed the propagation of artificially generated thermal pulse the in steel bars using infrared camera to locate the presence of cracks.

2   Thermal graphic imaging

Infrared is an electromagnetic radiation emits by all body above 0 K. The characteristic of the radiation depends on the temperature of the body so that the temperature of the body can be determined by the measured temperature. When an object is photographed using the infrared camera, the infrared radiation energy emitted by the object is received by the sensor of infrared camera and simultaneously converted to electronic signal. Then the electronic signal is processed by the controlling software to generate the thermal graphic image or, in short, thermograph.

Although to measure the absolute value of temperature with high precision using infrared camera requires robust and sophisticated calibration and strict control over atmospheric condition, the change in temperature can be detected remotely and non-intrusively on a large or small scale desired in specific scenario. Additionally, the thermograph also provide 2D geometry information which cannot be provided by other types of thermal sensors. Therefore, infrared camera is used in this research to detect crack formation in frozen soil in this research.

3   Experimental apparatus setup

In this research uniaxial compression test are conducted on frozen soil specimens while the specimens

are subjected to an infrared camera. The arrangements of the experimental apparatus are shown in Figure 1.
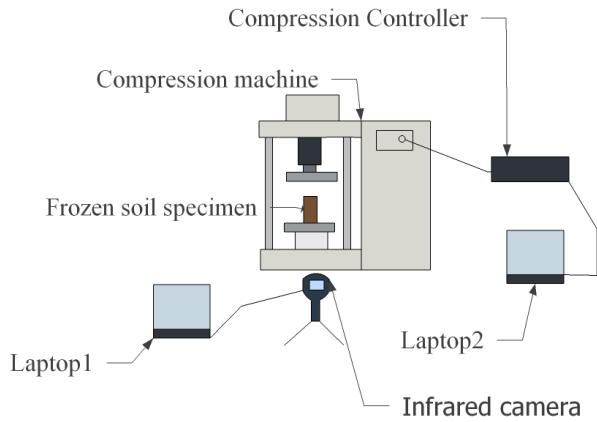
Figure 1. Experimental apparatus setup

The infrared camera is place approximately 1 m in front of the compression machine. The load is recorded at a frequency of 10 Hz. The Time-load curve is visible simultaneously on the laptop2 controlling the compression machine. The uniaxial compression test is terminated when the specimen fails or the lift of piston reached its capacity.

3.1 Specimen preparation

Three cases of soil category are considered in this study, namely clay, sand and gravel. For the clay specimen. The undisturbed clay sample extracted from 3 meters depth is cut into a cylinder of 100 mm (diameter) by 150 mm (height). And then submerged in a water tank for 24 hours to reach saturation. Afterwards it is put in the freezer for at least 24 hours. For the Sand and gravel cases, the soil particles and water are poured into moulds iteratively to make sure the specimen is fully saturated and composition relatively uniform across the height. Then they are frozen in a freezer before removed from the mould. Afterwards, the specimen are again stored in the freezer for 24 hours before test. Figure 2 shows process to make the frozen sand specimen.

Figure 2. Preparation of frozen soil specimen

Due to mechanical disturbance during the removal of the specimen, the height of sand and gravel specimen are not strictly controlled. The geometric information of specimens are shown is Table 1Figure 3 and the photos of specimens taken before the uniaxial compression tests are shown in Figure 3.

Table 1. Geometry of specimens

Material	Height (mm)	Diameter (mm)
clay	150	100
sand	171	100
gravel	179	100

(a)   (b)   (c)
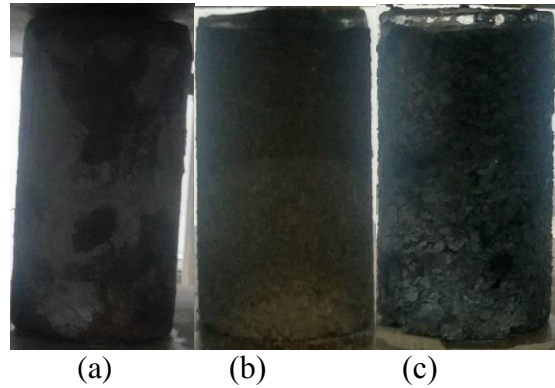
Figure 3. Frozen clay (a) sand (b) and gravel (c) specimens before uniaxial compression tests

3.2 Infrared camera

The infrared camera used is Flir E60.When an object is photographed using the infrared camera, the infrared radiation energy emitted by the object is received by the sensor of infrared camera and simultaneously converted to electronic signal. Then the electronic signal is processed by the Flir R&D controlling software to generate the temperature profile. The exported results file consists sequence of thermographic photos taken at a frequency of 30 Hz and resolution of 320*240 pixels. Each pixel in a frame has its temperature measured. The exported thermographic files are analysed using software Flir Research IR. The thermal sensitivity is 0.05°C and accuracy is ±2°C.

4 Result and Analysis

Due to lack of pre-existing knowledge of what and how a crack would appear in thermograph of frozen soils. The thermographs were carefully examined frame by frame. The qualification of a crack can be qualitatively described as follows:

- Significant temporal temperature variation, comparing to the immediate surrounding area (baseline), occurs at certain spots of relatively small area.

- The temperature variation initiates within the specimen surface and is not transmitted from the interface between specimen and ambient environment.
- The temperature variation is sustained more than 1 frame, which disqualifies those false positives caused by random flocculation in measured value of temperature.
- The temperature variation is not caused by mass transportation i.e. movement of disintegrated soil particle or water flow thawed from ice.

4.1 Crack in frozen clay

As shown in the load-time curve in Figure 4, the load peaks at 96.30 s after test started.
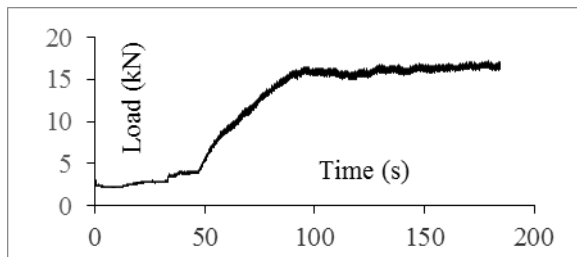
Figure 4. uniaxial load-time curve of clay specimen

After 96.30 s, temperature of certain points on the specimen surface appears to increase at a slightly higher rate than that of the rests. One example is indicated in **Error! Reference source not found.** as the crack point. A baseline point about 4 mm downwards of the crack point is selected to mitigate the effect of measurement error and the effect of heating from the ambient atmosphere on the variation of temperature.
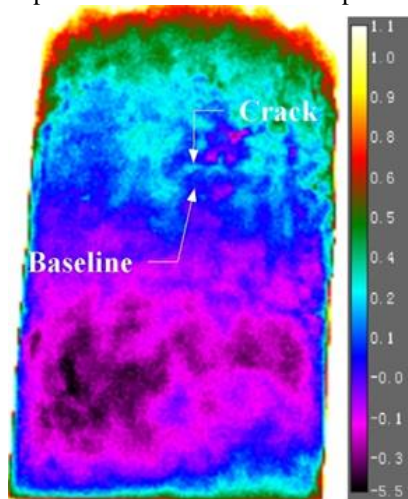
Figure 5. Temperature profile of clay specimen

The temperature-time curve for the crack point and baseline point are plotted in Figure 6. Disregarding the random flocculation, from 105 s to 123s seconds, the T increases from -3.02 °C to -2.41 °C. The temperature increase at crack point is further verified by the temperature profile along a line approximately perpendicular to the crack as shown in Figure 7. Temperature profile at the start of the test (0 s), immediately before the crack occurs (105 s), and after the crack forms (125 s), are plotted. Before the crack occurs, there is no significant difference in temperature between potential crack point and the rest. After the crack is formed, the temperature at the crack point is 0.57°C higher than those at points not influenced by the crack.
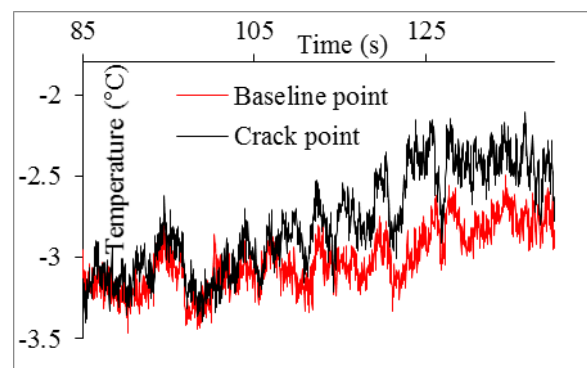
Figure 6. Temperature-time curve of crack point and baseline
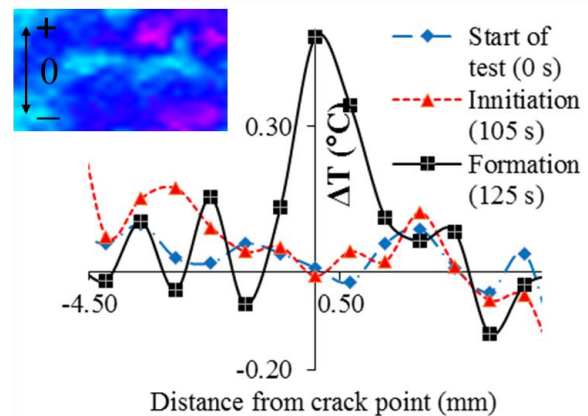
Figure 7. Temperature profile along a measurement line approximately perpendicular to the crack (the position of the measurement line is marked on the temperature profile attached on the top left)

4.2 Bulge effect in frozen sand

Although there is no individual crack observed in the sand case. As the frozen sand specimen is compressed,

the. The expansion in radial direction, which we call bulge, becomes significantly visible after yield and the phenomenon can also be correlated to temperature variation. The temperature of three representative points located at upper part (U.), lower left part (L.L), lower right part (L.R), and average temperature of a square area (S.) are selected to demonstrate the effect of bulge on temperature. The locations are indicated in Figure 8.
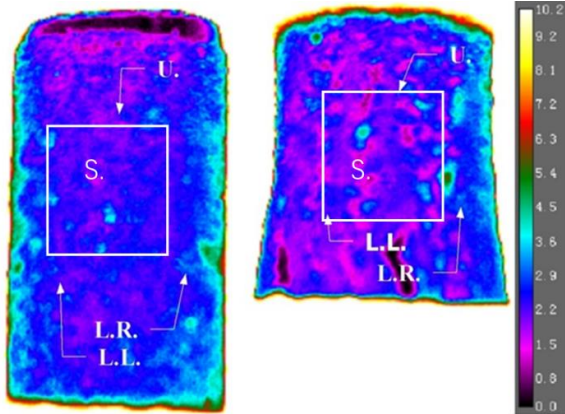
Figure 8. Temperature profile of frozen sand specimen at start (left) and end (right) of compression test

.

The temperature and load curves are plotted together in Figure 9. As the bulge of the specimen becomes obvious after yield (64.9 s), the temperature of every single point of specimen surface demonstrate 4 simultaneous impulsive increase initiating at 66.80 s, 88.30 s, 99.53 s and 110.30 s respectively. Impulses are not observed at points outside of the specimen surface, which means these impulses are not measurement error. The magnitude of ΔT for the impulses ranges from 0.37 to 0.95 °C.
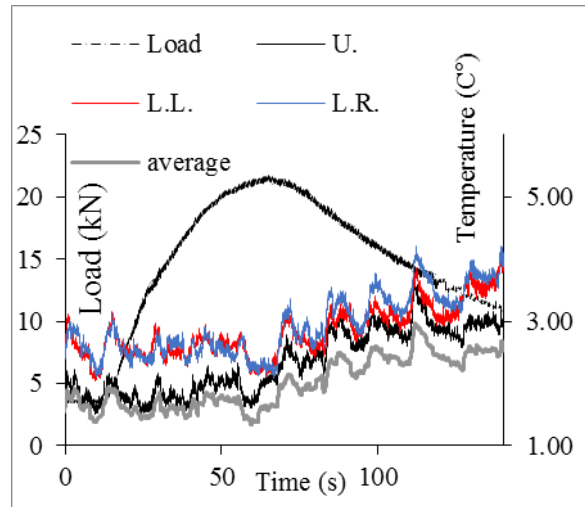
Figure 9. Load curve and temperature-time curve of sand specimen

4.3 Cracks in frozen gravel

Two types of cracks are observed during the compression test of the gravel specimen. The cracks, which occur in-between gravel particles, cause increases of temperature at crack point. Such cracks are noted as I1, I2 I3, and I4 following the initial of the word 'increase'. Temperature decrease at crack point is observed for cracks occur within ice block. Such cracks are noted as D1, D2, D3, D4, D5 and D6 following the initial of word 'decrease'. The ideal temperature variations for cracks of type I and D are illustrated in Figure 10. When cracks occur between gravel particles, the inter-particle friction generates heat. But those friction is relatively negligible between ice surfaces due to its smoothness. Even though there were heat generated around ice particles. The heat would probably be consumed by melting of ice rather than cause temperature increase. The temperature decrease is due to the temperature gradient from the surface to the inner core of specimen. When crack widens, the inner surface of the specimen, the temperature of which is lower comparing to the outside, is exposed to the camera. The location of these two types of cracks are indicated Figure 11.
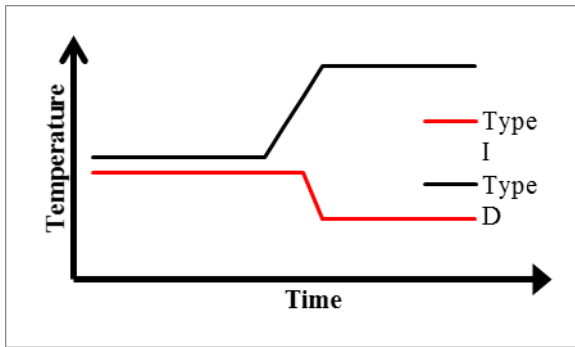
Figure 10. Ideal temperature-time curves of crack type I and type D
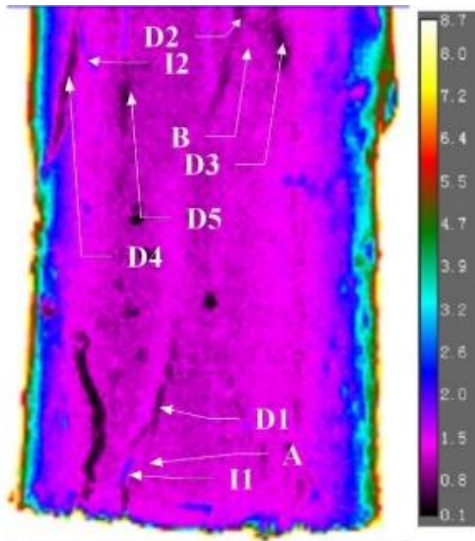
(a)
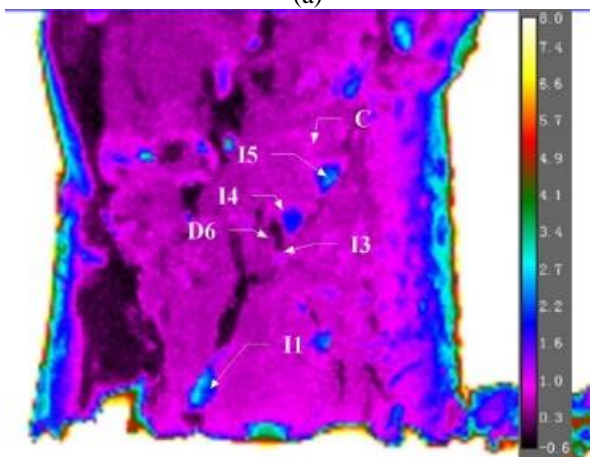
(b)

Figure 11. Locations of cracks before plastic deformation (a) and after plastic deformation (b)

Temporal variation for crack I1, D2 and D5 are Shown in Figure 12. Crack I1 occurs at the time of yield.

Before crack initiates, temperature of the crack point is relatively constant and approximately equals to the temperature of baseline. The T-t curve of crack point deviates from that of the baseline since t=126.33 s. From t= 126.33 to t=128.80s, the temperature at crack point increase by 0.6 °C while that at the baseline is relatively stable. After the crack is formed the temperature at the crack is relatively steady from 128.90 to 135.33 s but subsequently decreases due to the decrease of load. Crack D2 forms at the transitional point between stress softening and plastic deformation, which takes less time than the formation of crack I1. It is compatible with the common sense that the ice is very brittle and there was little friction. The magnitude of temperature decrease is not as important as the temperature increase for crack between gravel particles as the decrease only show how deep the crack develops into the specimen. The crack I5 occurs along the global failure surface during plastic deformation. The crack occurs at 265 s with a temperature increase of 0.51 ° C. After the relative movement between two parts of specimen on each side of the failure surface starts at 280 s the temperature increase takes 3 steps, which is corresponding to the steps of relative movement along the failure surface observed in the video. The load, and hence the stress within the specimen, is less than those previously during the elastic stage when I1 occurs. But the relatively movement along the global failure surface is more intense. Thus, both the rate of increase and total amount of increase in temperature is larger. From 280s to 315s, the temperature increase due to friction along the global failure surface is 2.66 °C.

(a)

(b)

(c)
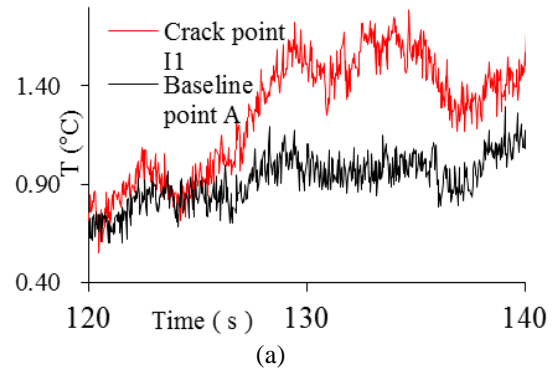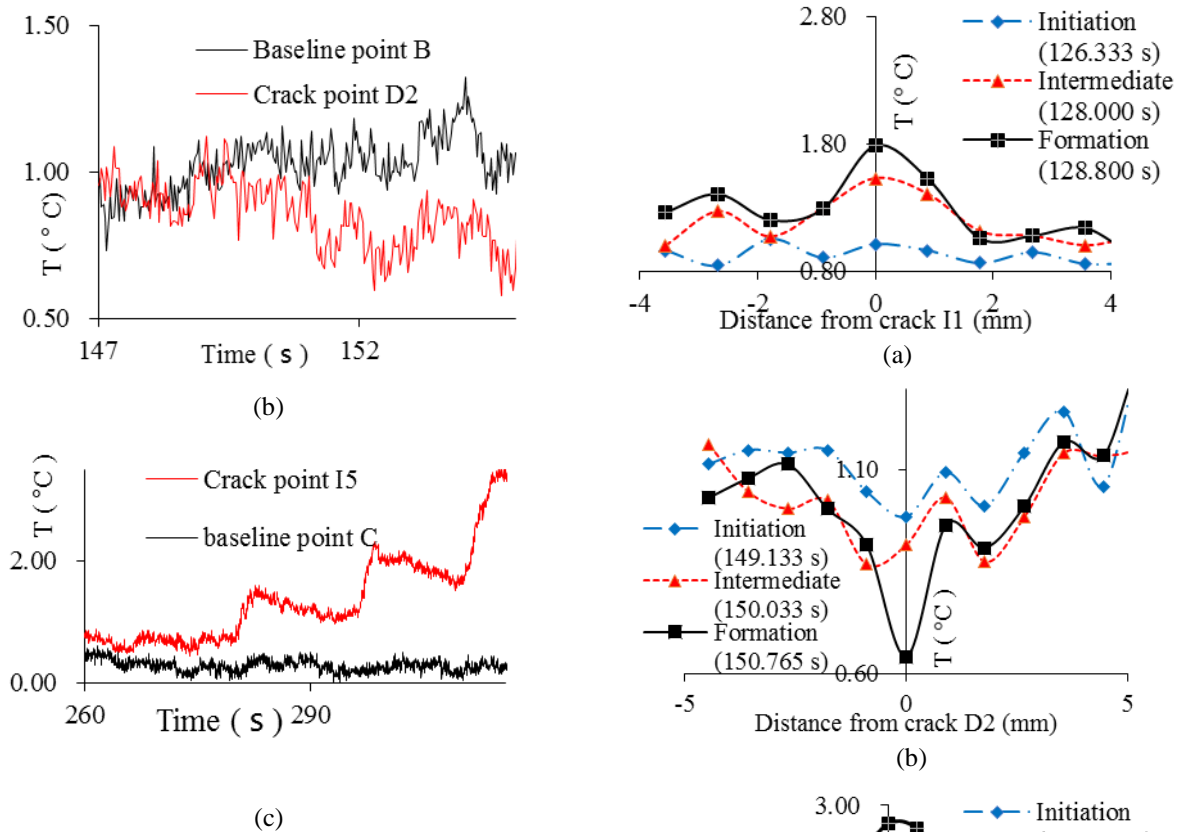
Figure 12. Temporal temperature variation at crack I1, D2, and I5 and their respective baseline A, B, and C.

The spatial temperature distribution across I1, D2, and I5 are also plotted to demonstrate the increase during the formation of crack in Figure 13. ΔT_{I1} is defined as $\Delta T_{I1} = T_{I1} - T_{average}$,where T_{I1} is the temperature at crack I1 at formation and $T_{average}$ is the average at the immediate surrounding area of crack I1.In the same manner, the time t_i, when the crack is fully developed, and ΔT_i is recorded for cracks I2, I3, I5, D1, D3, D4, and D6. After a crack has formed, the temperature may still vary subjected to the change in stress-strain condition. Thus the ΔT for crack I1 at stress-softening stage (noted by the initial 's' as subscript in $I1_s$) and plastic stage (noted by the initial 'p' as subscript in $I1_p$) and ΔT for Crack I2 at plastic stage are also calculated.

(a)

(b)

(c)
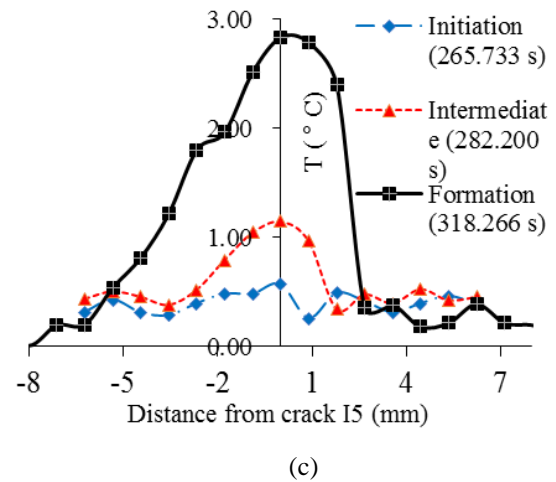
Figure 13. Temperature profile across crack I1, D2, and I5 during its formation

The serie of $(t_i, \Delta T_i)$ are plotted together with load-time curve in Figure 14. During the elastic stage, only two cracks, I1 and D1, occur slightly before yield (128.9 s). As the load decreases during the stress-softening period, the ΔT at crack I1 also decreases. A series of crack consisting 4 type D and 1 type I occur just before the transition to plastic deformation at 162.0 s. Afterwards, the load is relatively constant as the compression reached its plastic stage and no crack occurs until t=265 s, when the cracks later forming the global failure line initiates. From t= 265 s to t 300s, the global

failure surfaces gradually grow by connecting these individual cracks and the temperature along it generally increases. The total temperature increases at this series of cracks are all above 2.1 °C.
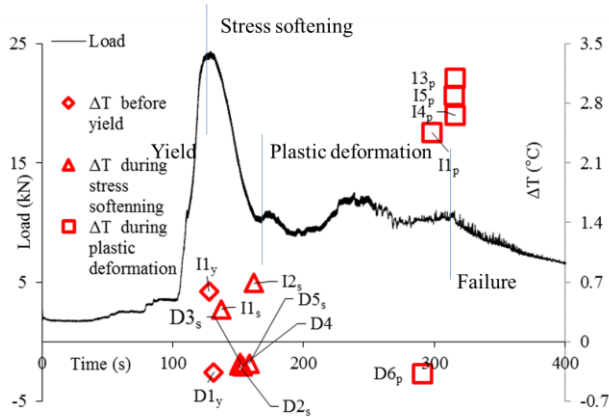
Figure 14. Load-time curve with magnitudes of temperature change at cracks

5   Conclusion

In this research, the thermographic profile of frozen soil specimen under uniaxial compression test is studied. For all 3 cases, abnormal temperature variations on specimen surface due to inter-particle friction occur are observed.

1.   In frozen clay specimen, the temperature increases at cracks are identified only after plastic deformation occurs
2.   For the frozen sand, simultaneous temperature increases are observed on the entire specimen as it bulges at plastic stage.
3.   In frozen gravel, temperature change are observed at cracks before and after yield. For cracks in ice particles, temperature decreases due to change in geometry. For cracks in gravel particles temperature increases due to inter-particle friction.

6   outlook

In this research, the identification of temperature change induced by friction is achieved after the thermal-videos are manually examined for multiple times and the temperature variation at manually selected points are analysed. Such manual observation and analysis are time-consuming and not efficient enough for real-time monitoring. Thus, the application of this method for monitoring on-site requires significant improvement in efficiency in the future.

Reference

[1]   PilŽIs, K. and V. VaiŠIs, DETECTION OF OIL product ON THE WATER SURFACE WITH thermal INFRARED camera. Naftos aptikimas vandens paviršiuje naudojant infraraudonųjų spindulių kamerą., 2017. 9(4): p. 357-362.
[2]   Fukuhara, T., et al., Detection of Small Wildfire by Thermal Infrared Camera With the Uncooled Microbolometer Array for 50-kg Class Satellite. IEEE Transactions on Geoscience and Remote Sensing, 2017. 55(8): p. 4314-4324.
[3]   Hagen, N., Passive imaging of wind surface flow using an infrared camera. Infrared Physics & Technology, 2017. 87: p. 47-54.
[4]   Seo, H., et al., Crack Detection in Pillars Using Infrared Thermographic Imaging. Vol. 40. 2017. 20150245.
[5]   Broberg, P., Surface crack detection in welds using thermography. NDT & E International, 2013. 57: p. 69-73.
[6]   Štarman, S. and V. Matz, Automated System for Crack Detection Using Infrared Thermographic Testing. 2012.